China Ocean Eng., 2017, Vol. 31, No. 3, P. 330–340
DOI: 10.1007/s13344-017-0039-9, ISSN 0890-5487
http://www.chinaoceanengin.cn/ E-mail: coe@nhri.cn

Effect of Peak Perforation on Flow Past A Conic Cylinder at *Re*=100: Drag, Lift and Strouhal Number

LIN Li-ming*, ZHONG Xing-fu, WU Ying-xiang

The Key Laboratory for Mechanics in Fluid Solid Coupling Systems, Institute of Mechanics, Chinese Academy of Sciences, Beijing 100190, China

Received April 20, 2016; revised November 16, 2016; accepted December 15, 2016

Abstract

A flow past a circular-section cylinder with a perforated conic shroud, in which the perforation is located at the peak of the conic disturbance as the shroud installed on the cylinder and uniformly distributed with several circular holes, is numerically simulated at a Reynolds number of 100. Two factors in the perforation are taken into account, i.e. the attack angle relative to the direction of incoming flow and diameter of holes. The effect of such perforation on the drag, lift and vortex-shedding frequency is mainly investigated. Results have shown that variation of the attack angle has a little effect, especially on the drag and vortex-shedding frequency, except in certain cases due to the varied vortex-shedding patterns in the near wake. The increasing hole diameter still exhibits a little effect on the drag and frequency of vortex shedding, but really reduces the lift, in particular at larger wavelength, such as the lift reduction reaching almost 66%–68% after introducing the perforation.

Key words: vortex-induced vibration, perforation, conic disturbance, drag, lift, Strouhal number

Citation: Lin, L. M., Zhong, X. F., Wu, Y. X., 2017. Effect of peak perforation on flow past a conic cylinder at *Re*=100: drag, lift and Strouhal number. China Ocean Eng., 31(3): 330–340, doi: 10.1007/s13344-017-0039-9

1 Introduction

Bluff bodies are commonly used in many engineering applications, for instance mooring cables, flexible risers and pipelines between the oil platform and submarine drilling well, cables in suspension bridges, and heat exchangers. When the flow passes bluff bodies, vortices are generated on surfaces due to the fluid viscosity and shed alternatively behind bodies. It is important because such phenomenon gives rise to unsteady loading, which further leads to the structural vibration, called vortex-induced vibration (VIV). Especially when synchronization occurs for vortex-shedding frequency close to natural frequency of structural oscillation, the sudden amplification in structural amplitude, as well as fluid forces, results in structural fatigue failure and integrity damage. Therefore, a great number of experimental and numerical investigations have been carried out to understand the dynamics of VIV in recent decades. Comprehensive reviews on this subject have been given in the literature (Sarpkaya, 2004; Williamson and Govardhan, 2004, 2008; Gabbai and Benaroya, 2005).

On the other hand, eliminating the vortices alternatively shedding from bluff bodies, alleviating the unsteady fluid loadings and then suppressing VIV to improve structural validity are also significant. Therefore, many methods have been proposed over half a century and mainly attributed to control the wake dynamics. For example, on the cylinder surface, the control bump spirally distributed around the cylinder (Owen et al., 2001) reduces the drag about 47%. At a certain wave steepness, defined by the ratio of the wave height to the wavelength of wavy disturbance, there is not any more sign of vortex shedding in the near wake. Such device is mainly effective in the higher mass-damping parameter. The triple-starting helical grooves on surfaces (Huang, 2011) are also found to be effective in suppressing VIV with the peak-amplitude reduction of 64%. Drag reduction of up to 25% is achieved in the subcritical Reynolds numbers. In the boundary layer of the cylinder, two small rotating cylinders can delay the separation of the boundary layer away from the cylinder's surface (Korkischko and Meneghini, 2012). The drag reduction reaches up to almost 60%. Around the cylinder, multiple control rods are used in suppressing VIV of slender flexible riser with the length to diameter ratio of 175 (Wu et al., 2012). Displacements in both cross and in-line flows are reduced almost 90% with the minimum spacing ratio of 0.187. The dominant mode and end tension are slightly increased due to the existence of

Foundation item: This work was financially supported by the National Key Scientific Instrument and Equipment Development Program of China (Grant No. 2011YQ120048).

*Corresponding author. E-mail: llmbirthday@163.com

control rods. The ventilated trouser (VT) as an entirely new and innovative quasi-fairing for VIV suppression of cylindrical structures has been proposed and investigated recently (King et al., 2013). The VT is a loose fitting sleeve in the form of a light flexible net with integral bobbins. Recently, a traveling wave wall as a kind of shape control method has been proposed to suppress VIV (Xu et al., 2014). A series of small-scale vortices would be formed in the troughs of the traveling wave on the rear of cylinder, which could effectively control the flow separation and eliminate the oscillating wake. Generally speaking, the streamline fairing (Lee and Allen, 2005) exhibits a very good aerodynamic performance due to the streamlined outer shape and the resultant of the delay of flow separation. It could also be achieved through installing (free-to-rotate) two-dimensional (2-D) splitter plates (Assi et al., 2009; Huera-Huarte, 2014). The largest drag reduction is about 60%. Along the riser's span, helical strake (Trim et al., 2005; Korkischko and Meneghini, 2010) is the most widely used way presently to disturb the spanwise uniformity of vortex shedding. More information about them or other passive control methods can be found in review works (Sarpkaya and Isaacson, 1981; Kumar et al., 2008; Wu and Sun, 2009).

Lately, another VIV suppressing method has been proposed by introducing three-dimensional (3-D) geometric disturbance, such as a wavy front surface (Bearman and Owen, 1998) and totally wavy cylinders with invariant circular- or square- sections (Owen et al., 1999; Darekar and Sherwin, 2001; Lin et al., 2010). Effect of such wavy disturbance would be sensitive to specific incoming flow direction because it is introduced in a streamwie-spanwise plane. To be omni-direction, radial disturbance introduced in a radial-spanwise plane was thus proposed (Lin et al., 2011), such as harmonic, spheroidal, ellipsoidal, conic and conic-like disturbances. It should be emphasized here that these radial disturbances are installed outside the straight cylinder as a kind of VIV shroud. Among them, the harmonic disturbance has been investigated through experimental measurements of its wake and numerical simulations by large-eddy simulations (LES) (Zhang et al., 2005; Lam and Lin, 2008, 2009), which really reduces drag and lift within a certain range of parameters. Meanwhile, experimental results for VIV of pendulum with harmonic and conic-like disturbances in water channel (Lin et al., 2012) have shown that the oscillating amplitude is reduced greatly at the start of lock-in, but increased at a higher reduced velocity. This indicates that the frequency of vortex shedding from cylinders with these disturbances is reduced in comparison with that without disturbances, verified lately by numerical simulations (Lin et al., 2013, 2014b). Because of the intrinsic difference between pendulum and riser, the flow past the fixed circular cylinder with harmonic and conic disturbances was numerically simulated at the Reynolds number of 100 (Lin et al., 2013, 2014a). Results have shown that variations of hydrodynamic parameters, vortex patterns in the near wake and other flow characteristics are qualitatively similar for such two disturbances with varied wavelength and wave steepness. Subsequently, the flow past the cylinder with the conic disturbance is further investigated at other subcritical Reynolds numbers (10^3, 10^4 and 10^5) (Lin et al., 2014b, 2015). Generally, the drag is gradually increased as the wave steepness increases, while the lift is firstly reduced quickly and then increased gradually. The frequency of vortex shedding is gradually decreased with the increasing wave steepness.

Based on the conic disturbance above, an improvement is adopted for initial goals, further trying to reduce the drag and lift forces as much as possible. On the basis of previous work (Lin et al., 2014a), the time-averaged pressure at the peak of conic disturbance is obviously greater than that at the valley; and the increase of drag is mainly attributed to the greatly increasing projected area due to the introduction of conic disturbance. In addition, the straight, circular-section and perforated shroud has been already proposed as a kind of methods in suppressing VIV over thirty years reported in a literature (Sarpkaya and Isaacson, 1981). Thus, such kind of improvement, the perforation on the conic shroud, is applied with several holes uniformly distributed at the peak of shroud (Lin et al., 2015). Results have shown that in a certain range of control parameters, the drag is really reduced a little, while the lift is reduced greatly with the change of vortex-shedding patterns in the near wake.

In the present paper as one of a series of works, the main purpose is to qualitatively investigate the effect of such perforation on the drag, lift and frequency of vortex shedding at the Reynolds number of 100. Two factors, the attack angle due to the specific direction of holes relative to the direction of incoming flow and diameter of holes, are considered. This paper is organized as follows. The numerical simulations, including the physical model and numerical methods and so on, are presented at first. Then results of the effect of both factors are given in detail. Finally the conclusions are made in brief.

2 Numerical simulations

2.1 Physical model

As shown in Fig. 1, an incompressible flow with the constant density ρ and kinematic viscosity ν past two kinds of circular-section cylinders is taken into account. Among them, one as shown in Fig. 1a introduces the conic disturbance along the span into the straight circular cylinder, referred to as the conic cylinder (marked by a letter of 'C' in the following figures), and another in Fig. 1b is obtained by introducing perforation at the peak of conic disturbance with several circular holes uniformly distributed along the azimuthal direction on the basic conic cylinder, referred to as

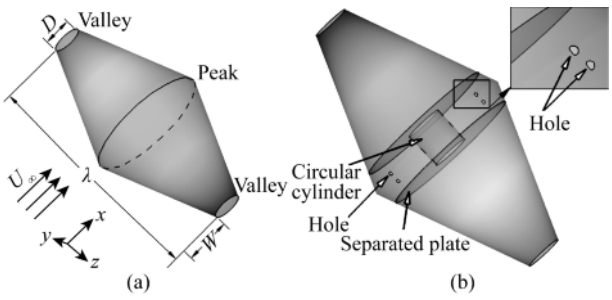

Fig. 1. Schematics of flows past (a) a conic cylinder and (b) the conic cylinder with introduced perforation at the peak.

the perforated conic shroud or cylinder (marked by letters of 'Co'). The basic conic disturbance can be mathematically described by the wavelength λ, the peak-to-valley wave height W and the base diameter D. Correspondingly, the peak and valley are defined as spanwise positions with maximal and minimal diameters, i.e. $(2W+D)$ and D, respectively. Thereby, the straight circular cylinder without the conic disturbance can be obtained by reducing W down to zero. Besides, the diameter of holes Do, their number No and attack angle Ag between the central axis of the hole near the front stagnation point of the cylinder and incoming flow are used to describe the introduced perforation.

In present flow fields, the inertial Cartesian coordinate system (x, y, z) is established. The x-axis, referred to as the streamwise direction, is aligned with the free upstream flow with the uniform velocity U_∞. The z-axis, referred to as the spanwise direction, is aligned with the central axis of the cylinder. While the y-axis, referred to as the vertical direction, is perpendicular to the (x, z) plane.

The non-dimensional continuity and Navier–Stokes equations governing present flows are then obtained as:

$$\nabla \cdot \boldsymbol{u} = 0; \tag{1}$$

$$\frac{\partial \boldsymbol{u}}{\partial t} + (\boldsymbol{u} \cdot \nabla)\boldsymbol{u} = -\nabla p + \frac{1}{Re}\nabla^2 \boldsymbol{u}, \tag{2}$$

where $\boldsymbol{u}=(u, v, w)$ is the velocity vector, p is the static pressure, t is the non-dimensional time by U_∞ and D, ∇ is the gradient operator and Re is the Reynolds number, $Re=U_\infty D/v$. Lengths are scaled by the base diameter D and velocities by the free-stream velocity U_∞.

In a temporally periodic flow, the frequency of the vortex shedding, f, is non-dimensionalized as the Strouhal number, defined by $St=fD/U_\infty$.

The fluid force, drag and lift, are normalized by the free-stream dynamic pressure and the projected area of the body A, i.e. $\rho U_\infty^2 A/2$, to produce the force coefficient. For the convenience of comparisons of these fluid forces between the straight cylinder and the cylinder with conic disturbance or perforated conic shroud (it should be emphasized here that the drag of perforated conic shroud includes drags of shroud, separated plates and central cylinder), the projected area (A) must be computed from the straight cylinder with the same spanwise length, that is $A=\lambda D$, instead of the conic cylinder or perforated conic shroud themselves. In the following context, C_{D_M} and C_{L_RMS} are the mean drag coefficient and the root-mean-square (RMS) lift coefficient, respectively.

2.2 Boundary conditions

In order to obtain the appropriate numerical solutions, the boundary conditions should be properly proposed. To simulate flows around cylinders with an infinite spanwise length, it is commonly adopted that the flow is assumed to be periodical along the spanwise direction. Then as for the boundary conditions in the (x, y) plane, the uniform free-stream velocity ($\boldsymbol{u} = (U_\infty, 0, 0)$) at the inlet, simple non-reflecting outflow ($\partial \boldsymbol{u}/\partial x=0$) at the outlet, free slip ($\partial(u, w)/\partial y=v=0$) at the vertical sides and non-slip boundary condition ($\boldsymbol{u}=0$) on cylinder surfaces are prescribed. Reference pressure is zero at the inlet with $y=0$.

2.3 Computational domain and grid

It is also very important that the proper size of the computational domain should be carefully selected to weaken its effect on the flow field, fluid forces and vortex shedding frequency as much as possible. Based on previous work (Lin, 2007) and present computational resources and costs in time, the non-dimensional computational domain in the (x, y) plane is 40×20 $(x\times y)$, as shown in Fig. 2. The dimensionless computational length in the z-axis is given as one period of the conic disturbance, i.e. λ/D.

Different from the structural grids in a hexahedral form for a straight or conic cylinder, mesh generation for the perforated conic shroud is more complicated due to the appearance of circular holes at the peak of the conic disturbance. Typical mesh distributions in the (x, y) plane are shown in Figs. 2a and 2b. Far away from the cylinder, the hexahedral grids are also adopted and coarsened (It should be explained here that in Fig. 2b those unlike hexahedral grids upstream are actually resulted from intersections of a sectioned plane $z=\lambda/(2D)$ and oblique hexahedral grids). While in the flow region near the cylinder, where the distance of regional boundary away from the cylinder surface is $2D$ in the x and y directions, and holes, the unstructured grids in forms of triangle on the surface and tetrahedron in space are applied and concentrated. As shown in Figs. 2c and 2d, the finest non-dimensional grid spacing is of order $O(10^{-2})$ on the front stagnation surface and $O(10^{-3})$ on the rear surface. As for different wavelength of the cylinder, the dimensionless grid spacing in the spanwise direction is at most 0.1. Then the total number of spanwise grids is greater than $10\lambda/D$, such as 60 for $\lambda/D=6$. Hence, total numbers of 3-D grids are approximately $(4–6)\times10^5$, $(5–8)\times10^5$ and $(0.6–1.2)\times10^6$ for $\lambda/D=4$, 6 and 8, respectively.

The measured maximum values for skewed elements are

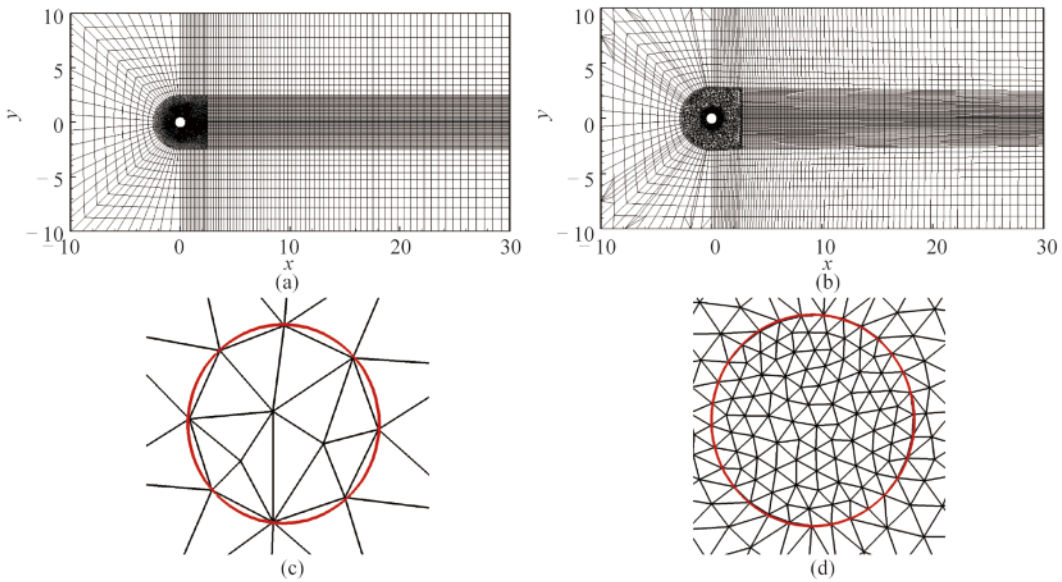

Fig. 2. Non-dimensional computational domain and typical grid distributions at (a) z=0 and (b) z=λ/(2D), and mesh for the holes (red line) near (c) the front and (d) rear surfaces.

0.8–0.85. Numbers for these higher skewed elements are usually not more than 10–30. Most of them are distributed upstream near the boundary between the structural and unstructured grids, so they have little effects on the flow near the cylinder and the near wake.

2.4 Numerical methods

Numerical simulations for present flow evolution are carried out by the commonly-used commercial fluid computation software, FLUENT. Due to the laminar flow at Re= 100, the laminar viscous model is applied. Details of numerical methods are presented with the aim of the result verification, computation repeatability and future improvement.

As for the time discretization, the second order is used with a non-dimensional time step of 0.01. In controlling the discretization of the convection terms in the solution equations, the second order scheme for the pressure and the second order upwind scheme for the momentum are selected.

In software, the Green–Gauss node-based method is considered for computing the gradient of the scalar at the cell center.

In computing the pressure-velocity coupling equations, the SIMPLEC algorithm is adopted with zero skewness correction (default value).

After applying the multiple-grid method, the flexible cycle type is chosen with aggregative AMG (algebraic multi-grid) solver for stabilization for all equations.

The maximal convergence residual reaches the lower order of $O(10^{-4})$ for the continuity equation, and $O(10^{-5})$ for three components of the momentum equations.

2.5 Control parameters and verification of computations

Except the Reynolds number as the typical control parameter for the present flow, there are some other parameters mainly describing the conic disturbance for conic cylinders and circular holes for perforated conic shroud. Firstly as for the conic disturbance, two independent length parameters, the non-dimensional wavelength λ/D and the wave steepness W/λ are obtained to describe the similarity between different conic cylinders. Then as for the perforation, the non-dimensional diameter of holes Do/D, number of holes No and attack angle Ag, are the main control parameters. Therefore, in the present simulated flow, there are six control parameters for the perforated conic shroud, constituting a large parameter space.

In the present study, a series of computational investigations were carried out. Based on previous studies (Lin et al., 2014b) at various subcritical Reynolds numbers, the effect of increasing Reynolds number is little on the qualitative variation of the drag, lift and St in flows past the conic cylinder. As a fundamental research, the Reynolds number is still set to be 100 in order to keep the flow laminar without introducing the effect of different turbulent models at higher Reynolds numbers. Various dimensionless wavelengths λ/D are 4, 6 and 8. Different wave steepness W/λ is 0.0125, 0.025, 0.05, 0.1 and 0.2. Diameters of circular holes Do are varied from 0.1D, 0.2D to 0.4D. Only four holes are computed (the effect of increasing number of holes would be investigated in future work). Because of the symmetry of the perforation with four holes, the attack angles Ag are then presented to be 0°, 15°, 30° and 45°.

Two points should be mentioned here. The first is the result of the straight circular cylinder as a basic case to be presented at data points of W/λ=0 in the following figures. The second is the special parameter groups composed of Do

and *Ag*. For example, when *Do*/*D* is varied, only *Ag*=0° is considered; or only the cases at *Do*/*D*=0.1 are computed as the increasing *Ag*.

It is necessary to verify the above numerical methods before presenting the simulated results, although they have already been reported in previous works (Lin et al., 2013, 2015). The first verification is the basic case of 2-D flow past the straight circular cylinder at *Re*=100. As shown in Fig. 3, the wake topology is typically identified as the well-known Kármán vortex. As shown in Table 1, it is in a good agreement for the drag and lift coefficients and *St* between the present simulations and previous experimental and numerical results (Sarpkaya and Isaacson, 1981; Henderson, 1997; Newman and Karniadakis, 1997).

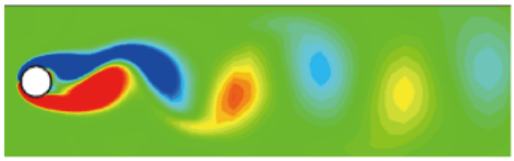

Fig. 3. Contours of the spanwise vorticity in the basic case describing the Kármán vortex shedding at *Re*=100, where the red and blue colors of contours denote the positive and negative values of spanwise vorticity respectively. Note that the cylinder is shown by a wire frame (same as follows).

Table 1 Comparisons of C_{D_M}, C_{L_RMS} and *St* between the present calculation and previous experimental and numerical results for the basic case

	C_{D_M}	C_{L_RMS}	*St*
Present	1.39	0.256	0.165
Experimental	1.25–1.4; 1.8	–	0.164
Numerical	1.37	0.24[a]	0.167

[a] It is evaluated from the maximum lift coefficient in the paper (Newman and Karniadakis, 1997).

In the second verification, two separated plates with a spanwise distance of 0.5*D* away from the peak are used, as shown in Fig. 1b. One of the reasons is that the flow in the inter-layer, the region between the inner straight cylinder and the conic shroud, is very weak with the order of velocity about $O(10^{-2})U_\infty$, especially close to the region of the valley. Another is to reduce the computational grids and save times. Nevertheless, the effect of such plates on the flow is still taken into account for a specific case (*λ*/*D*=8, *W*/*λ*=0.1, *Do*/*D*=0.1, *No*=4, *Ag*=0°) and compared with that without these plates. As shown in Table 2 (which rectifies a mistake for misplaced items of *St* and C_{D_M} in the previous paper (Lin et al., 2015), the application of separated plates has almost little effect.

Table 2 Comparisons of C_{D_M}, C_{L_RMS} and *St* for the case with and without separated plates at *λ*/*D*=8, *W*/*λ*=0.1, *Do*/*D*=0.1, *No*=4, and *Ag*=0°

Have separated plates?	C_{D_M}	C_{L_RMS}	*St*
Yes	2.157	0.108	0.075
No	2.151	0.105	0.075

In the third verification to know the effect of the increasing number of total grids on 3-D computations, especially for the perforated conic shroud, the fine mesh by doubling number of the mesh nodes on all edges is adopted in the same previous case (*λ*/*D*=8, *W*/*λ*=0.1, *Do*/*D*=0.1, *No*=4, *Ag*=0°). The total number of the volume mesh increases from the present mesh of 6×10^5 to the fine mesh of 3.4×10^6. Simulation runs in the fine mesh take about 4 times the time in the present mesh per time step. In the fine mesh, C_{D_M}=2.153, C_{L_RMS}=0.086 and *St*=0.075. Compared with those in the present mesh, the time-averaged drag coefficient and vortex-shedding frequency in the fine mesh are unaffected, but the RMS lift coefficient is reduced about 20%. As shown in Fig. 4, the drag and lift coefficients are almost the same qualitatively in time histories, especially during a whole period of varied $C_D(t)$. At last, the results obtained from the present mesh are qualitatively acceptable in consideration of whole computational times and overestimated from the engineering point if the fluid force needs to be reduced in practice.

3 Results of introduced perforation

3.1 Effect of various attack angles of free stream

One of the initial purposes to introduce radial disturbances in suppressing vortex-induced vibrations (Lin et al., 2011, 2012) is to avoid the effect of various directions of ocean current on VIV suppressors. However, the introduction of the perforation with a limited number of holes

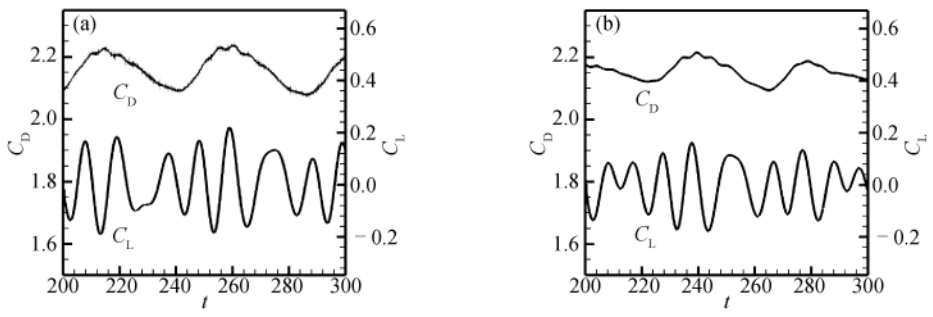

Fig. 4. Time histories of drag and lift coefficients in the case of *λ*/*D*=8, *W*/*λ*=0.1, *Do*/*D*=0.1, *No*=4 and *Ag*=0° for (a) present mesh and (b) fine mesh.

is naturally unavoidable to lead to the existence of such problem of incoming flow direction or the attack angle. Here we firstly focus on the effect of the perforation on hydrodynamic parameters varied along with the attack angle as follows.

As shown in Fig. 5, the results of variations of the mean drag coefficient C_{D_M} along with the non-dimensional wavelength λ/D, the wave steepness W/λ and the attack angle Ag for the flow past the perforated conic shroud are summarized. In general, the drag is almost linearly increased with the increasing wave steepness, and its increasing rate is also increased with the increasing wavelength. It has been shown that when Ag varies from 0° to 45°, the drag is almost equivalent to that without perforation, with relative variations of smaller than 2%–5% in most cases (except two cases: λ/D=4 and W/λ=0.1, and λ/D=8 and W/λ=0.2). In particular, in the case of λ/D=4 and W/λ=0.1, the drag at Ag=0° is much smaller than the drag without perforation and with increasing Ag>0°, which indicates that there is a sudden transformation of the pattern of vortex shedding in the near wake, as shown in Fig. 6 where Kármán vortex street is almost suppressed at Ag=0° but alternatively shed at Ag=15°. Anyhow, generally speaking, this illustrates that the incoming flow with different directions relative to the perforated conic shroud has almost no influence on the mean drag coefficient.

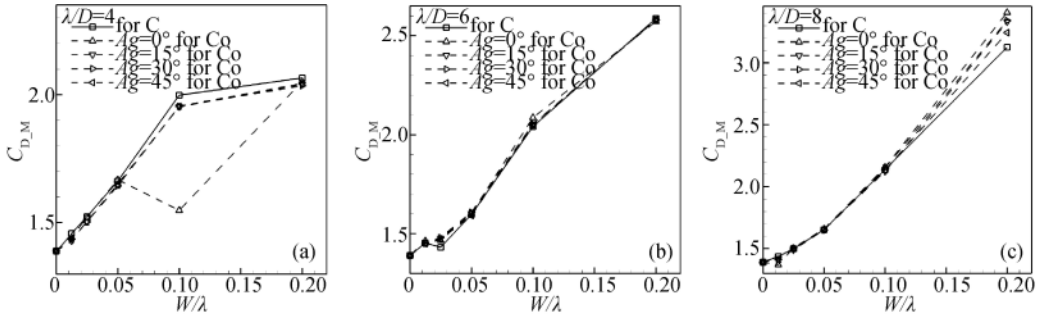

Fig. 5. Variations of the mean drag coefficient C_{D_M} along the wave steepness W/λ and the attack angel Ag at the non-dimensional wavelength of (a) λ/D=4, (b) 6 and (c) 8.

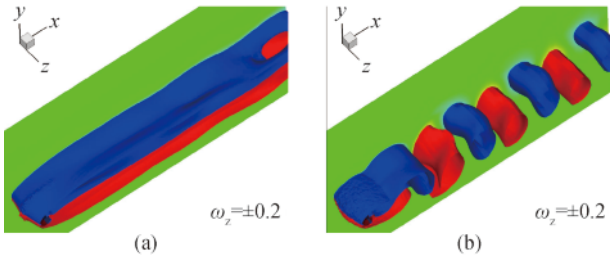

Fig. 6. Iso-surfaces of spanwise vorticity in the near wake for (a) Ag=0° at t=600 and (b) Ag=15° at t=550 in the case of λ/D=4 and W/λ=0.1 with Do/D=0.1, where the red and blue colors indicate the positive and negative values.

As shown in Fig. 7 or Fig. 8 (only for "Co"), the effect of different attack angles is apparent on the RMS lift coefficient C_{L_RMS}, distinguished from that on C_{D_M}. Generally as the wave steepness increases, the lift is firstly increased and then decreased at λ/D=4; while for cases at λ/D=6, the lift is reduced at first and then increased and until $W/\lambda \geqslant 0.1$, it is finally reduced; as for cases at λ/D=8, the lift is only first reduced and then increased. Especially, at cases of W/λ=0.2 with λ/D=4 and 6, C_{L_RMS} is almost invariable or uninfluenced by Ag.

Moreover, in cases with λ/D=4 and W/λ<0.1, C_{L_RMS} at Ag>0° is smaller than that at Ag=0° or those without the

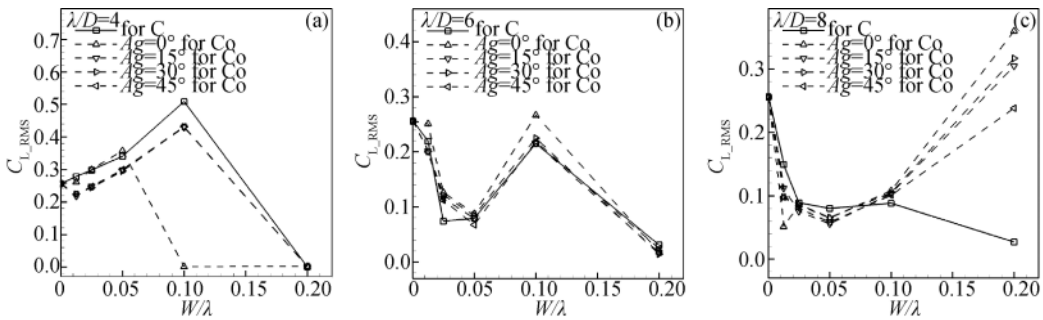

Fig. 7. Variations of the RMS lift coefficient C_{L_RMS} along the wave steepness W/λ and the attack angel Ag at the non-dimensional wavelength of (a) λ/D=4, (b) 6 and (c) 8.

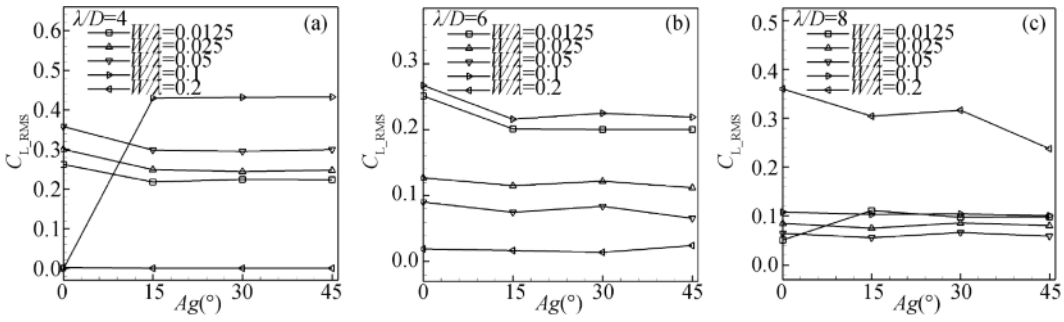

Fig. 8. The RMS lift coefficient C_{L_RMS} for 'Co' versus the attack angle Ag with different wave steepness W/λ at the non-dimensional wavelength of (a) λ/D=4, (b) 6 and (c) 8.

perforation. And C_{L_RMS} is almost invariant when Ag= 15°–45°. When λ/D is 6, the lift from W/λ=0.025 to 0.1 is greater than that without the perforation. Furthermore, the lift at Ag>0° is obviously smaller than that at Ag=0° when $W/\lambda \leqslant 0.1$. As λ/D increases up to 8, the lift with the introduced perforation is firstly smaller at W/λ<0.1 and then larger at $W/\lambda \geqslant 0.1$ than that without the perforation. The variation of C_{L_RMS} with W/λ[0.025, 0.1] is very little for different attack angles. The great increase of C_{L_RMS} at W/λ=0.2, even higher than that of the straight cylinder, also indicates the significant pattern transformation of vortex shedding, as shown in Fig. 9.

Generally speaking, from the point of engineering view, the application of perforation is recommended mainly at λ/D=8 with small W/λ.

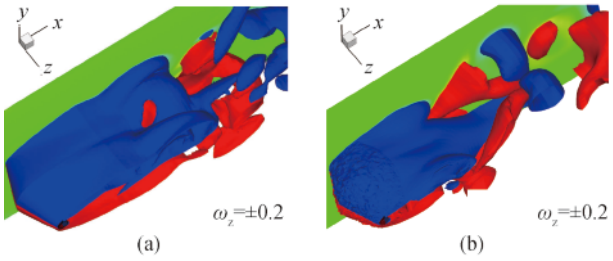

Fig. 9. Iso-surfaces of spanwise vorticity in the near wake for (a) the conic cylinder at t=850 and (b) the perforated conic cylinder at t=420 with Ag=0° and Do/D=0.1 in the case of λ/D=8 and W/λ=0.2, where the red and blue colors indicate the positive and negative values.

Fig. 10 presents the summary of the non-dimensional vortex shedding frequency along with λ/D, W/λ and Ag, that is the Strouhal number St at the highest power spectral density (PSD) obtained by the fast Fourier transform (FFT) to the time history of the lift coefficient. As the wave steepness increases, St gradually decreased. For most cases, the results have shown that St is less influenced by the variation of the attack angel and almost close to that without the perforation, similar to the behaviors of C_{D_M}. Particularly, as for the case of λ/D=4 and W/λ=0.1, the variation of St at different Ag certainly manifests the vortex behind the body totally suppressed at Ag=0° become alternatively shedding at other Ag>0°.

In brief, in most cases, the drag and vortex-shedding frequency are almost little affected, while the lift becomes a little greater or less than that without the perforation, as the attack angle increases.

3.2 Effect of increasing diameter of perforation

As reported in the previous paper (Bearman, 1967), the base bleed has been successfully used in the past to suppress vortex shedding and reduce the base drag. The effect of the base bleed, similar to the splitter plate (Roshko, 1955), is to delay the upper and lower separated shear layers interacting with each other and hence it increases the formation length, that is the position at which the vortices are fully formed, or the length of the time-average recircula-

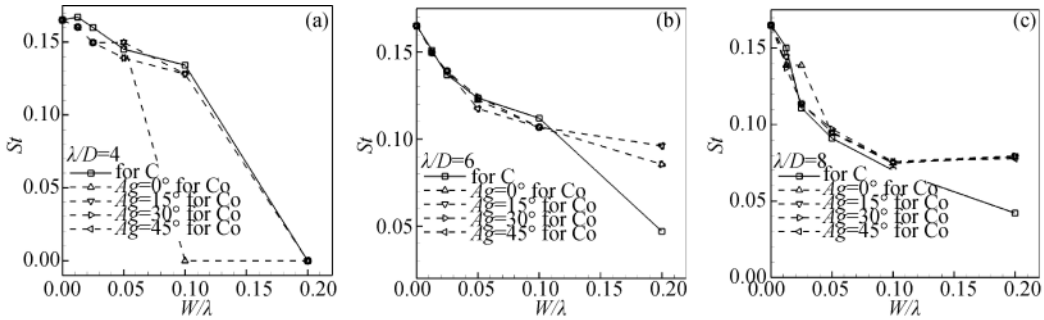

Fig. 10. Variations of the Strouhal number St along the wave steepness W/λ and the attack angel (Ag) at the non-dimensional wavelength of (a) λ/D=4, (b) 6 and (c) 8.

tion region. A recent numerical simulation shows that the windward suction combined with leeward blowing around the circular cylinder can eliminate the vortex shedding and consequently suppress VIV (Dong et al., 2008). With its extra energy consumption to maintain the necessary suction and/or blowing, a cylinder with a streamwise-oriented slit was then proposed and numerically studied, which was found to be the most effective in reducing the drag and lift forces (Baek and Karniadakis, 2009).

Based on these ideas, it seems to be reasonable and effective in reducing fluid forces by introducing the perforation at the peak of conic disturbance. However, through the above analysis at different attack angles or at least at Ag=0°, the effectiveness of the perforations looks like barely satisfactory. The reason might be that the diameter of the holes Do/D=0.1 is too small in the present circumstances to lead to the inside flow between the conic shroud and the straight cylinder strong enough to form the jet disturbing the near wake flow and vortex formation, just like what the slit in the cylinder does. With such curiosity, the investigation into the effect of the increasing diameter of the hole on fluid forces is carried out.

Fig. 11 presents the effect of increasing Do/D on C_{D_M}. Results have shown that as Do/D increases, the variation of drag in most cases is still very little, even compared with that of the cylinder without the perforation, similar to that by increasing Ag as mentioned above. As a result, C_{D_M} in most cases is also almost linearly increased as W/λ increases when the holes become bigger. Howbeit, through careful comparison with those results varied along Ag, the drag with the perforation varied with both Ag and Do is mainly smaller than that without the perforation at λ/D=4, larger at λ/D=6, and at λ/D=8 firstly smaller when W/λ<0.05 and then larger when $W/\lambda \geqslant 0.05$.

Results of C_{L_RMS} varied with the increasing Do/D are summarized in Fig. 12 or Fig. 13 (it should be mentioned here that results for the conic cylinder could be illustrated at Do/D=0). As the wave steepness increases, features of variation of the RMS lift coefficient with different Do/D are still similar to that with different Ag and without the perforation in most cases. Different from the effect of Ag, the variation of C_{L_RMS} is evident.

Generally, as Do/D increases, C_{L_RMS} in most cases is gradually decreased, among them if the one in the case of λ/D=4 and W/λ=0.1 could be assumed to be the value at Ag>0° as shown in Fig. 7a (for the comparison's sake, it is reasonable due to the flow at Ag=0° easily disturbed and diverted to other direction). As for λ/D=4, C_{L_RMS} with Do/D>0.1 is smaller than that without the perforation, similar to the variation due to Ag>0°. In the case of W/λ=0.2, the zero lift indicates the total suppression of the vortex shedding is unaffected by the increasing either Do/D or Ag. As λ/D is 6, C_{L_RMS} is firstly smaller at Do/D=0.1, then closer at Do/D=0.2 and finally smaller at Do/D=0.4 than that without the perforation. When λ/D increases up to 8, C_{L_RMS} is firstly all smaller than that without the perforation when

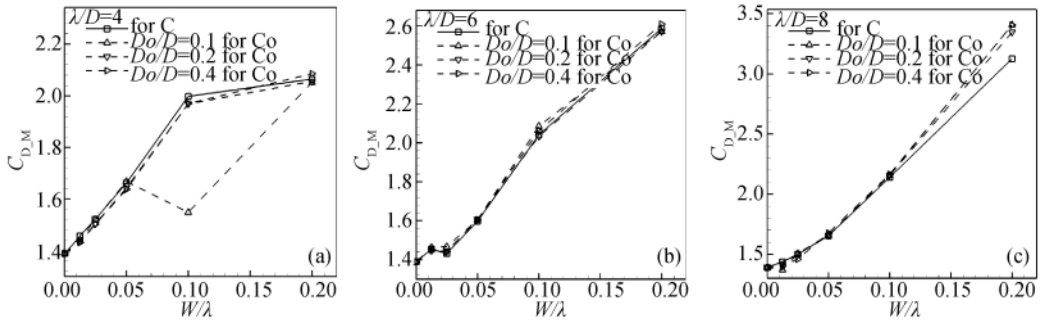

Fig. 11. Variations of the mean drag coefficient C_{D_M} along the wave steepness W/λ and the hole diameter Do at the non-dimensional wavelength of (a) λ/D=4, (b) 6 and (c) 8.

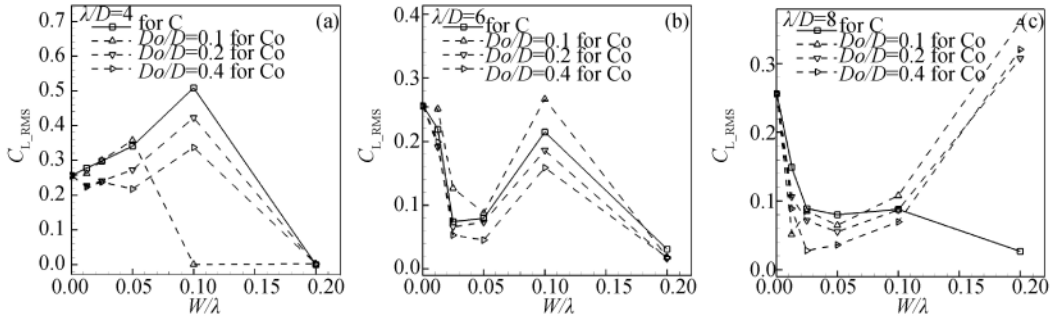

Fig. 12. Variations of the RMS lift coefficient C_{L_RMS} along the wave steepness W/λ and the hole diameter Do at the non-dimensional wavelength of (a) λ/D=4, (b) 6 and (c) 8.

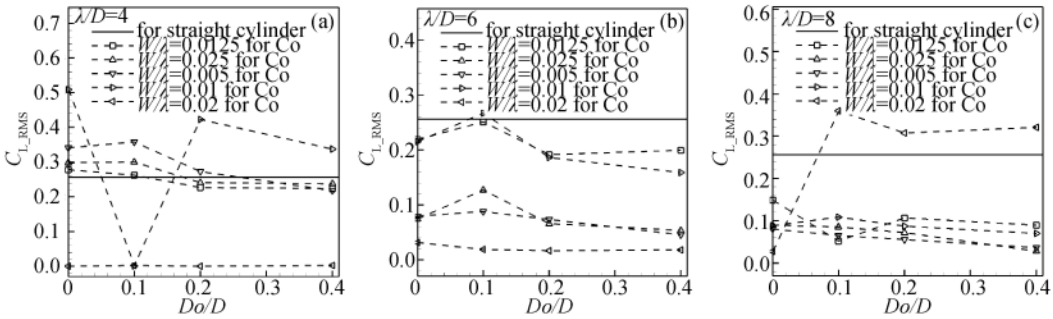

Fig. 13. The RMS lift coefficient C_{L_RMS} versus non-dimensional hole diameter Do/D with different wave steepness W/λ at the non-dimensional wavelength of (a) λ/D=4, (b) 6 and (c) 8.

W/λ<0.1 and then gradually becomes larger when $W/\lambda \geqslant 0.1$, just like what C_{L_RMS} varied along Ag does.

Therefore, based on the above behaviors of fluid forces, the parameter groups are suggested to be Do/D=0.4 at λ/D=8 with smaller W/λ, typically from 0.0125 to 0.05. For example, at the case of W/λ=0.0125 and Do/D=0.1, the drag is just a little reduced 1.4% to that of the straight cylinder and 4.5% to that of the conic cylinder without the perforation, but the lift is almost reduced about 80% and 66%, respectively. Or for the case of W/λ=0.025 and Do/D=0.4 the drag is increased within 5% but the lift is greatly reduced about 89% if compared with those of the straight cylinder, or the drag reduction is about 2.7% and the lift reduction about 68% when compared with those of the conic cylinder.

As shown in Fig. 14, it can be seen that the effect of varied Do on St is almost similar to that due to the varied Ag. As for cases with the increasing wave steepness, St is generally reduced. As Do/D increases, St is approximately equal to that without the perforation in most cases. Especially at the case of λ/D=4 and W/λ=0.1, the increase of Do/D also leads to the total suppression of the vortex shedding at Do/D=0.1 failed and the vortex in the near wake becomes alternatively shedding, although the attack angle still remained 0°. This further indicates that the status of the suppressed vortex shedding at the case of Do/D=0.1 is unstable, or there is a very little region in the parameter space of Do/D where the total suppression of alternatively shedding vortex could be realized. In the case of λ/D=4 and W/λ=0.2, the total suppression of the vortex shedding is strongly stable with the increase of Do/D or Ag. Besides, for cases at λ/D=8 and W/λ=0.025 and 0.05, the vortex shedding frequencies at Do/D=0.4 are remarkably greater than those at small Do/D and without the perforation, which may give us a hint that there exist different patterns of the vortex shedding in the near wake.

In a word, although variations of fluid forces and vortex-shedding frequency with the increasing diameter of perforation are quite similar to those because of the varied attack angle, obvious reduction in the RMS lift coefficient in most cases indicates that the adoption of larger diameter of the perforation, or at least in certain cases the introduction of the perforation, is of effectiveness.

4 Conclusions

In the present paper, flows past the perforated conic shroud, that is a new kind of VIV shroud installed on the outside of the circular-section cylinder in the form of the conic disturbance with introduced perforation uniformly distributed at the peak of such disturbance, are numerically simulated at the Reynolds number of 100. Effects of such introduced perforation on the drag, lift and vortex-shedding frequency or the Strouhal number are mainly investigated. Except for a given series of geometric parameters for the conic disturbance, i.e. the non-dimensional wavelength (λ/D=4, 6 and 8) and wave steepness (W/λ=0.0125, 0.025, 0.05, 0.1 and 0.2), variations of the attack angle (Ag=0°,

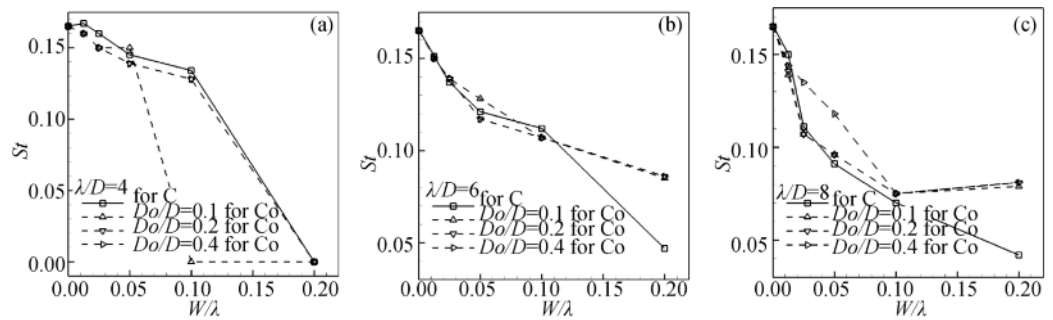

Fig. 14. Variations of the Strouhal number St along the wave steepness W/λ and the hole diameter Do at the non-dimensional wavelength of (a) λ/D=4, (b) 6 and (c) 8.

15°, 30° and 45°) and the dimensionless diameters of four circular holes (Do/D=0.1, 0.2 and 0.4) have been studied.

Overall, the present results have shown that the drag of the perforated conic shroud is hardly or little affected in most cases by the increasing attack angle (when Do/D=0.1) or the increasing non-dimensional hole diameter (when Ag=0°), and generally increased as W/λ increases. However, as the attack angle increases, although the variation of the lift is quantitatively obvious, such variation relative to the lift without the introduced perforation is almost unaffected qualitatively in most cases. Generally, the lift is greatly reduced when the diameter of the holes increases, especially for λ/D=6 and 8; in a certain case (λ/D=8, W/λ=0.025 and Do/D=0.4), the reduction reaches up to 68% compared with the lift without introduced perforation. This indicates that the increase of diameter of perforation is really effective in reducing the lift of the conic cylinder, even for the straight cylinder. As for the vortex-shedding frequency, the influences of the attack angle and the hole's diameter are quite little, except certain cases in which the pattern of the vortex shedding in the near wake is already transformed into other pattern.

Therefore, finite effect of different attack angles caused by the introducing perforation on the hydrodynamic parameters indicates that the application of the perforation is nearly omnidirectional. The increasing diameter of the perforation is of importance because it can further reduce the lift force efficiently at larger wavelength of conic disturbance.

In the next work, flow patterns, including the vortex shedding and other flow characteristics in the near wake of the perforated conic shroud, will be investigated with varied attack angles and diameters of the perforation, as well as frequency analysis by the wavelet. In future, researches on the effect of the increasing number of circular holes and the coverage of perforation randomly distributed on whole shroud for the perforated conic shroud and the coverage of conic shroud without perforation on the straight cylinder on patterns of vortex shedding and hydrodynamic parameters would be put on the next schedule.

References

Assi, G.R.S., Bearman, P.W. and Kitney, N., 2009. Low drag solutions for suppressing vortex-induced vibration of circular cylinders, *Journal of Fluids and Structures*, 25(4), 666–675.

Baek, H. and Karniadakis, G.E., 2009. Suppressing vortex-induced vibrations via passive means, *Journal of Fluids and Structures*, 25(5), 848–866.

Bearman, P.W., 1967. The effect of base bleed on the flow behind a two-dimensional model with a blunt trailing edge, *Aeronautical Quarterly*, 18(3), 207–224.

Bearman, P.W. and Owen, J.C., 1998. Reduction of bluff-body drag and suppression of vortex shedding by the introduction of wavy separation lines, *Journal of Fluids and Structures*, 12(1), 123–130.

Darekar, R.M. and Sherwin S.J., 2001. Flow past a square-section cylinder with a wavy stagnation face, *Journal of Fluid Mechanics*, 426, 263–295.

Dong, S., Triantafyllou, G.S. and Karniadakis, G.E., 2008. Elimination of vortex streets in bluff-body flows, *Physical Review Letters*, 100(20), 204501.

Gabbai, R.D. and Benaroya, H., 2005. An overview of modeling and experiments of vortex-induced vibration of circular cylinders, *Journal of sound and Vibration*, 282(3–5), 575–616.

Henderson, R.D., 1997. Nonlinear dynamics and pattern formation in turbulent wake transition, *Journal of Fluid Mechanics*, 352, 65–112.

Huang, S., 2011. VIV suppression of a two-degree-of-freedom circular cylinder and drag reduction of a fixed circular cylinder by the use of helical grooves, *Journal of Fluids and Structures*, 27(7), 1124–1133.

Huera-Huarte, F.J., 2014. On splitter plate coverage for suppression of vortex-induced vibrations of flexible cylinders, *Applied Ocean Research*, 48, 244–249.

King, R., Brown, A., Braaten, H., Russo, M., Baarholm, R. and Lie, H., 2013. Suppressing full-scale riser VIV with the VT suppressor, *Proceedings of ASME the 32nd International Conference on Ocean, Offshore and Arctic Engineering*, ASME, Nantes, France.

Korkischko, I. and Meneghini, J.R., 2010. Experimental investigation of flow-induced vibration on isolated and tandem circular cylinders fitted with strakes, *Journal of Fluids and Structures*, 26(4), 611–625.

Korkischko, I. and Meneghini, J.R., 2012. Suppression of vortex-induced vibration using moving surface boundary-layer control, *Journal of Fluids and Structures*, 34, 259–270.

Kumar, R.A., Sohn, C.H. and Gowda, B.H.L., 2008. Passive control of vortex-induced vibrations: an overview, *Recent Patents on Mechanical Engineering*, 1(1), 1–11.

Lam, K. and Lin, Y.F., 2008. Large eddy simulation of flow around wavy cylinders at a subcritical Reynolds number, *International Journal of Heat and Fluid Flow*, 29(4), 1071–1088.

Lam, K. and Lin, Y.F., 2009. Effects of wavelength and amplitude of a wavy cylinder in cross-flow at low Reynolds numbers, *Journal of Fluid Mechanics*, 620, 195–220.

Lee, L. and Allen, D.W., 2005. The dynamic stability of short fairings, *Offshore Technology Conference*, Offshore Technology Conference, Houston, Texas, USA.

Lin, L.M., 2007. *Wake Dynamics and Forces in the Flow around the Square-section Cylinder with a Geometric Disturbance*, Ph.D. Thesis, Institute of Mechanics, CAS, Beijing, China. (in Chinese)

Lin, L.M., Ling, G.C. and Wu, Y.X., 2010. Mechanism responsible for the complete suppression of Kármán vortex in flows past a wavy square-section cylinder, *Chinese Physics Letters*, 27(3), 034702.

Lin, L.M., Zhong, X.F. and Wu, Y.X., 2011. Experimental investigation of a new device in suppressing vortex-induced vibrations of a circular cylinder, *Proceedings of the 21st International Offshore and Polar Engineering Conference*, International Society of Offshore and Polar Engineers, Maui, Hawaii, USA, pp. 1283–1288.

Lin, L.M., Zhong, X.F. and Wu, Y.X., 2012. Vortex-induced vibrations of a circular cylinder with different geometric disturbances, *Proceedings of the 22nd International Offshore and Polar Engineering Conference*, International Society of Offshore and Polar Engineers, Rhodes, Greece, pp. 623–629.

Lin, L.M., Zhong, X.F. and Wu, Y.X., 2013. Flow around a circular cylinder with radial disturbances at a low Reynolds number, *Proceedings of the 23rd International Offshore and Polar Engineering Conference*, International Society of Offshore and Polar Engineers,

Anchorage, Alaska, USA, pp. 387–394.

Lin, L.M., Zhong, X.F. and Wu, Y.X., 2014a. Characteristics for a flow past a circular cylinder with two types of radial disturbances at *Re*=100, *Advanced Materials Research*, 871, 107–114.

Lin, L.M., Zhong, X.F. and Wu, Y.X., 2014b. The drag, lift and strouhal number of a circular-section cylinder with a conic disturbance at subcritical Reynolds numbers, *Proceedings of ASME 2014 the 33rd International Conference on Ocean*, *Offshore and Arctic Engineering*, ASME, San Francisco, California, USA.

Lin, L.M., Zhong, X.F. and Wu, Y.X., 2015. Effects of a higher Reynolds number and introduced perforation on flows past the conic cylinder, *Proceedings of the 25th International Ocean and Polar Engineering Conference*, International Society of Offshore and Polar Engineers, Kona, Big Island, Hawaii, USA, pp. 997–1003.

Newman, D.J. and Karniadakis, G.E., 1997. A direct numerical simulation study of flow past a freely vibrating cable, *Journal of Fluid Mechanics*, 344, 95–136.

Owen, J.C., Bearman, P.W. and Szewczyk, A.A., 2001. Passive control of VIV with drag reduction, *Journal of Fluids and Structures*, 15(3–4), 597–605.

Owen, J.C., Szewczyk, A.A. and Bearman, P.W., 1999. Suppressing Kármán vortex shedding by use of sinuous circular cylinders, *Bulletin of the American Physical Society*, 44, 124.

Roshko, A., 1955. On the wake and drag of bluff bodies, *Journal of the Aeronautical Sciences*, 22(2), 124–132.

Sarpkaya, T. and Isaacson, M., 1981. *Mechanics of Wave Forces on Offshore Structures*, Van Nostrand Reinhold Company, New York.

Sarpkaya, T., 2004. A critical review of the intrinsic nature of vortex-induced vibrations, *Journal of Fluids and Structures*, 19(4), 389–447.

Trim, A.D., Braaten H., Lie, H. and Tognarelli, M.A., 2005. Experimental investigation of vortex-induced vibration of long marine risers, *Journal of Fluids and Structures*, 21(3), 335–361.

Williamson, C.H.K. and Govardhan, R., 2004. Vortex-induced vibrations, *Annual Review of Fluid Mechanics*, 36(1), 413–455.

Williamson, C.H.K. and Govardhan, R., 2008. A brief review of recent results in vortex-induced vibrations, *Journal of Wind Engineering and Industrial Aerodynamics*, 96(6–7), 713–735.

Wu, H. and Sun, D.P., 2009. Study on suppression measures for vortex-induced vibration of the deepwater riser, *China Offshore Platform*, 24(4), 1–8. (in Chinese)

Wu, H., Sun, D.P., Lu, L., Teng, B., Tang, G.Q. and Song, J.N., 2012. Experimental investigation on the suppression of vortex-induced vibration of long flexible riser by multiple control rods, *Journal of Fluids and Structures*, 30, 115–132.

Xu, F., Chen, W.L., Xiao, Y.Q., Li, H. and Qu, J.P., 2014. Numerical study on the suppression of the vortex-induced vibration of an elastically mounted cylinder by a traveling wave wall, *Journal of Fluids and Structures*, 44, 145–165.

Zhang, W., Daichin. and Lee, S.J., 2005. PIV measurements of the near-wake behind a sinusoidal cylinder, *Experiments in Fluids*, 38 (6), 824–832.